Research Square

Preprints are preliminary reports that have not undergone peer review.
They should not be considered conclusive, used to inform clinical practice,
or referenced by the media as validated information.

The growth characteristics and metabolic profiling of Δ 5,7 -sterols and fatty acids in Schizochytrium sp. S31 under different culture conditions

Xiao-Yu Zhang
Sun Yat-Sen University
Pei-Shan He
Guangzhou City Polytechnic
Yi-Nan Liao
Sun Yat-Sen University
Juan Peng
pengj28@mail.sysu.edu.cn

Sun Yat-Sen University
Jian-Ping Yuan
Sun Yat-Sen University
Jun Zhao
Sun Yat-Sen University

Research Article

Keywords: Schizochytrium, Δ5,7-sterols, Astaxanthin, Docosahexaenoic acid, Fatty acids

Posted Date: November 5th, 2026

DOI: https://doi.org/10.21203/rs.3.rs-11424938/v1

License: This work is licensed under a Creative Commons Attribution 4.0 International License.
Read Full License

Additional Declarations: No competing interests reported.

Abstract

Schizochytrium is a promising thraustochytrid cell factory for co-producing high-value bioactives; however, its growth and bioactive accumulation depend heavily on culture conditions. This study systematically investigated the growth characteristics and the changes in $\Delta^{5,7}$-sterols, fatty acids and astaxanthin of *Schizochytrium* sp. S31 under different concentrations of glucose (0–120 g/L), sea salt (0–130 g/L) and pH (3.5–7.5). Sea salt exerted a markedly stronger influence on sterol profiles and fatty acid contents than glucose or pH. Low salinity (10 g/L), with ergosterol constituting the largest proportion (41%), maximized total fatty acid (41.3% DCW) and DHA (7.3% DCW) contents, whereas higher salinities shifted sterol composition toward C28-$\Delta^{5,7}$ and increased trace astaxanthin levels. The maximum cell dry weight of 17.4 g/L was obtained at 60 g/L glucose, 20 g/L sea salt and pH 5.5, which was also the optimum condition for the simultaneous accumulation of $\Delta^{5,7}$-sterols (50.73 mg/L), docosahexaenoic acid (DHA, 1097 mg/L) and astaxanthin (0.11 mg/L). Transcriptomic analysis revealed a crosstalk among sterol, DHA and astaxanthin biosynthetic pathways in *Schizochytrium* sp. S31, and low salinity enhanced fatty acid β-oxidation to elevate the acetyl-CoA supply toward the mevalonate (MVA) pathway, while downregulating crtI and crtR to suppress downstream astaxanthin accumulation. Additionally, candidate genes involved in key phytosterols synthesis were identified. These findings provide critical insights into the biosynthetic regulation of sterols, astaxanthin, and DHA in thraustochytrids, highlighting their potential for the co-production of these high-value bioactives.

1. Introduction

Thraustochytrids are a group of unicellular, heterotrophic eukaryotic protists. They are ubiquitously distributed across diverse marine environments, including coastal seawater, sediments, mangrove ecosystems, and deep-sea marine snow (Jiang et al., 2020; Kalidasan et al., 2021). While conventionally grouped under “microalgae”, these non-photosynthetic heterotrophic organisms act as indispensable decomposers, nutrient recyclers, and carbon sink contributors in marine ecosystems (Bochdansky et al., 2017; Lee Chang et al., 2012). Beyond their ecological importance, thraustochytrids have attracted growing industrial interest as sustainable cell factories capable of the biosynthesis of high-value bioactive compounds, including omega-3 long-chain polyunsaturated fatty acids, carotenoids, and sterols (Song et al., 2024).

As a typical thraustochytrid, members of the genus *Schizochytrium* exhibit rapid heterotrophic growth and synthesize very long-chain polyunsaturated fatty acids (VLCPUFAs), predominantly docosahexaenoic acid (DHA) (Peng et al., 2025), which making them a versatile microbial source for nutraceutical, feed, and aquaculture applications (Xie et al., 2020; Shi et al., 2021; Chi et al., 2022; Permanasari et al., 2026). Moreover, their capacity for recombinant protein expression makes *Schizochytrium* an emerging host for oral vaccine delivery platforms (Ramos-Vega et al., 2018). However, the growth dynamics and intracellular metabolite biosynthesis of *Schizochytrium* are significantly influenced by culture conditions, particularly carbon source concentration, salinity, and pH, and these responses are highly strain-specific. For instance, *Schizochytrium* sp. G13/2S grows well at high glucose

concentrations of 100–200 g/L (Ganuza et al., 2008), whereas early investigations on *Schizochytrium* sp. S31 identified an initial glucose concentration of 28 g/L in the basal medium as optimal for DHA synthesis (Wu and Lin, 2003). Strains from distinct ecological niches also exhibit contrasting salinity adaptations. The estuarine strain *Schizochytrium* sp. FJ-1 maintains relatively high biomass at 5 g/L sea salt, whereas the marine strain *Schizochytrium* sp. 20888 (S31) exhibits a prolonged lag phase and poor growth performance under the same conditions (Ye et al., 2025). Meanwhile, the proportion of DHA in total fatty acids for *Schizochytrium limacinum* OUC88 increased as salinity decreased from 36 to 9 (Zhu et al., 2007). Regarding pH, early work revealed that neutral conditions (pH 7.0) maximized both biomass and DHA accumulation in S31 (Wu and Lin, 2003), whereas lipid synthesis in *Schizochytrium* sp. AB-610 was enhanced under acidic conditions (pH 5.0) during the late fermentation phase (Zhao et al., 2017). Notably, a recent meta-analysis indicated that thraustochytrids maintained stable PUFA biosynthesis across a broader pH range of 5.0 to 8.0 (Da Costa et al., 2026).

Beyond fatty acid synthesis, the metabolic potential of *Schizochytrium* extends to other high-value bioactive molecules. Specifically, we recently identified high-value astaxanthin as the primary carotenoid in *Schizochytrium* sp. S31, alongside four distinct $\Delta^{5,7}$-sterols, including ergosterol, ergosta-5,7-dien-3β-ol (C28-$\Delta^{5,7}$), ergosta-5,7,24(28)-trien-3β-ol (C28-$\Delta^{5,7,24(28)}$) and 24-ethylcholesta-5,7,22-trien-3β-ol (C29-$\Delta^{5,7,22}$) (Jiang et al., 2020). Among these, ergosterol serves as provitamin D_2, while C28-$\Delta^{5,7}$ has been characterized as a precursor to vitamin D_4. Crucially, $\Delta^{5,7}$-sterols are well-established structural components of eukaryotic cell membranes, as demonstrated by the finding that replacing ergosterol with fecosterol in *Saccharomyces cerevisiae* alters membrane physical properties and confers thermotolerance (Caspeta et al., 2014). Membrane sterols also regulate plasma membrane mechanical stability under hyperosmotic stress, thereby enhancing cellular osmotolerance (Dupont et al., 2011). However, limited research has focused on the dynamic responses of sterols in the thraustochytrid *Schizochytrium* under varying culture conditions. Whether environmental factors—such as carbon source concentration, salinity, and pH—modulate these intracellular metabolites (e.g., sterols and astaxanthin) to mediate physiological acclimation in *Schizochytrium* remains largely unexplored.

On the other hand, given its proven ability to co-accumulate $\Delta^{5,7}$-sterols, astaxanthin, and DHA (Jiang et al., 2020), *Schizochytrium* has strong potential for the development of high-value functional ingredients with multi-functional benefits. However, current research and industrial applications of *Schizochytrium* have predominantly focused on optimizing DHA yield. In green microalgae, a tight metabolic synergy often exists between carotenoid and lipid biosynthesis; for instance, inhibiting de novo fatty acid biosynthesis markedly reduced or suppressed astaxanthin accumulation in *Haematococcus pluvialis* cells, and a positive correlation between astaxanthin and fatty acid synthesis was observed in photoautotrophic and heterotrophic *Chromochloris zofingiensis* (Zhang et al., 2019). Conversely, in certain thraustochytrids, culture conditions promoting carotenoid biosynthesis were found to conflict with squalene accumulation (Koopmann et al., 2023). Whether metabolic competition or biosynthetic divergence exists among $\Delta^{5,7}$-sterol, astaxanthin, and DHA pathways in *Schizochytrium*, or whether their simultaneous co-accumulation can be achieved, remains unclarified. Consequently, the potential for

driving the simultaneous co-production of these three bioactive compounds in *Schizochytrium* under varying fermentation regimes has yet to be fully explored.

Therefore, this study investigated the growth characteristics and changes of $\Delta^{5,7}$-sterols, astaxanthin and fatty acids of *Schizochytrium* sp. S31 under varying culture conditions. Single-factor experiments were conducted to evaluate the effects of glucose (0–120 g/L), sea salt (0–130 g/L) and pH (3.5–7.5). Cell morphology, dry cell weight (DCW), and the contents of $\Delta^{5,7}$-sterols, astaxanthin, total fatty acids, and DHA were systematically evaluated. Furthermore, transcriptome sequencing was performed to elucidate the transcriptional regulatory patterns and metabolic interactions among these biosynthesis pathways. The findings provide foundational data and theoretical insights for optimizing multi-product co-production strategies in *Schizochytrium* and advance our understanding of lipid and terpenoid biosynthetic regulation in thraustochytrids.

2. Materials and Methods

2.1. Chemicals

Ergosterol (98% purity) and astaxanthin (97% purity) standards were purchased from Acros Organics (Geel, Belgium) and Sigma-Aldrich (St. Louis, MO, USA), respectively. Heptadecanoic acid (C17:0; Sigma-Aldrich) was used as the internal standard for fatty acid quantification. HPLC-grade methanol was purchased from CNW Technologies GmbH (Duesseldorf, Germany). For transcriptomic analysis, TRIzol reagent was acquired from Invitrogen (Carlsbad, CA, USA) and the TruSeq RNA Library Prep Kit along with HiSeq X Reagent Kits were supplied by Illumina (San Diego, CA, USA). Methanol (HPLC grade) was obtained from Merck (Darmstadt, Germany). All other chemicals were of analytical grade and obtained from local commercial suppliers. Deionized water was used throughout all experiments.

2.2. Strain and culture conditions

Schizochytrium sp. S31 (ATCC 20888) was obtained from the Guangdong Microbial Culture Collection Center (GDMCC) and stored at − 80°C in 40% (v/v) glycerol (prepared by mixing the culture broth with a 60% glycerol solution at a 1:2 volume ratio). The seed medium contained 50 g/L glucose, 2 g/L peptone, 5 g/L yeast extract and 35 g/L sea salt. For strain activation, the glycerol stock was inoculated into 4 mL of seed medium in a 10-mL screw-cap centrifuge tube and incubated at 25°C and 150 rpm for 30 min. The activated culture was subsequently transferred into a 250-mL Erlenmeyer flask containing 60 mL of seed medium and cultivated under the same conditions. On day 4, 4 mL of this culture was subcultured into 60 mL of fresh seed medium and grown for an additional 72 h. The resulting exponential-phase culture served as the inoculum for all subsequent experiments.

To evaluate the effect of glucose concentration, the basal medium (2 g/L peptone, 5 g/L yeast extract, and 20 g/L sea salt) was supplemented with glucose at concentrations of 0, 10, 20, 30, 40, 50, 60, 70, 80, 90, 100, 110 and 120 g/L. For sea salt optimization, the medium comprised 60 g/L glucose, 2 g/L peptone, and 5 g/L yeast extract, with sea salt concentrations varied at 0, 5, 10, 20, 30, 40, 50, 60, 70, 80,

90, 110, and 130 g/L. For pH optimization, the basal medium contained 60 g/L glucose, 2 g/L peptone, 5 g/L yeast extract, and 10 g/L sea salt, with the initial pH adjusted to 3.5, 4.5, 5.5, 6.5, and 7.5 using 3 M NaOH or HCl. Unless otherwise stated, the pH of all media was adjusted to 6.5 prior to autoclaving at 121°C for 20 min. These single-factor experiments were conducted in 250-mL Erlenmeyer flasks containing 60 mL of medium with a 5% (v/v) inoculum. All cultures were incubated at 25°C in a ZWYR-G2401 orbital shaking incubator (Zhicheng Analysis Instrument Manufacturing Co., Ltd., Shanghai, China) at 150 rpm for 6 days. All experimental treatments were performed in three independent biological replicates.

2.3. Microscopic observation and cell harvesting

After 6 days of cultivation under varying culture conditions, the cell morphology of *Schizochytrium* sp. S31 was examined using an optical microscope (BK-FL; Chongqing Scope Optics Instruments Co., Ltd., Chongqing, China) at 400× and 1000× magnifications.

For cell harvesting, a 1-mL aliquot of homogeneous culture broth was transferred into a pre-weighed 2-mL grinding tube and centrifuged at 10,000 rpm for 5 min. The resulting supernatant was collected for residual glucose measurement. The cell pellet was washed by resuspending in 0.5 mL of deionized water followed by centrifugation at 11,000 rpm for 5 min; this washing step was performed three times in total. The washed cells were stored at − 80°C for subsequent sterol and astaxanthin determination. The remaining culture in the flask was centrifuged at 4,000 rpm for 8 min, and the harvested cell pellets were pooled into a pre-weighed 50-mL screw-cap centrifuge tube. The collected cells were washed with an appropriate amount of deionized water and centrifuged at 4,000 rpm for 12 min for a total of three washes. The final cell pellet was frozen and stored at − 80°C until further analysis.

2.4. Determination of dry cell weight and residual glucose

The frozen cell pellets were lyophilized in a freeze dryer (Alpha 2–4 LSCplus, Martin Christ, Osterode, Germany) at 0.01 mbar for 48 h. Dry cell weight (DCW) was determined gravimetrically.

Residual glucose in the culture supernatant was quantified using the 3,5-dinitrosalicylic acid (DNS) method (Miller, 1959). The DNS reagent was prepared by dissolving 75 g of potassium sodium tartrate in deionized water with heating, followed by adding 16 g of NaOH and 1 g of 3,5-dinitrosalicylic acid, and the solution was brought to a final volume of 1 L and stored in the dark for 7 days before use. For the assay, 1 mL of appropriately diluted sample was mixed with 5 mL of DNS reagent and heated in a boiling water bath for 10 min. After cooling to room temperature, the absorbance was measured at 570 nm. Glucose concentration was calculated from a standard curve (R^2 = 0.9996) prepared with glucose standards in the range of 0–1 g/L.

2.5. Determination of $\Delta^{5,7}$-sterols and astaxanthin

$\Delta^{5,7}$-Sterols and astaxanthin were extracted and analyzed following the method described by Jiang et al. (2020). Dried cells were mixed with approximately 0.23 g of ceramic and glass beads in a 2-mL grinding

tube, and 1 mL of methanol was added as the extraction solvent. Cell disruption was performed with a bead mill homogenizer (Bead Ruptor 24, OMNI International, Kennesaw, GA, USA) at 4 m/s for 30 s with 1-min intervals (3 cycles per program). Five programs were executed in total, with the tubes cooled on ice for 1.5 min between programs. After grinding, the samples were vortexed for 20 s, ultrasonicated at 100% power for 10 min, and vortexed again for 20 s. This sonication step was repeated three times. The extract was centrifuged at 12,000 rpm for 10 min, and the supernatant was filtered through a 0.22-μm PTFE syringe filter prior to UPLC analysis.

UPLC analysis was carried out on a Waters ACQUITY UPLC H-Class system equipped with a PDA eλ detector (Waters, Milford, MA, USA). Separation was performed on a Waters CORTECS C18 column (2.7 μm, 2.1 × 75 mm) maintained at 30°C. The mobile phase was composed of water (A) and methanol (B) delivered at 0.4 mL/min. The gradient program started with 30% A and 70% B for 0.5 min, followed by 100% B from 0.5 to 7.0 min. The injection volume was 5 μL. $\Delta^{5,7}$-Sterols were monitored at 280 nm, and astaxanthin was monitored at 480 nm. Quantification was based on external standard curves of ergosterol and astaxanthin. The calibration curves were linear over 0.3–60 mg/L for ergosterol (A = 21497C, R^2 = 0.999) and 0.02–5 mg/L for astaxanthin (A = 35289C, R^2 = 0.9992).

2.6. Fatty acid analysis

Fatty acid extraction and transesterification were performed according to Zhang et al. (2019). with minor modifications. Freeze-dried cells were ground to a fine powder, and approximately 10 mg was weighed into a 25-mL screw-cap glass tube. Subsequently, 2 mL of 1% (v/v) H_2SO4 in methanol, 1 mL of BHT (80 mg/L in toluene) and 0.4 mL of C17:0 internal standard (1 g/L in hexane) were added. The mixture was ultrasonicated for 10 min and then incubated in a 50°C water bath for 14 h. After cooling to room temperature, 5 mL of saturated NaCl solution was added and the mixture was allowed to separate. The organic phase was extracted twice with 5 mL of hexane containing BHT (80 mg/L). The combined organic extracts were pooled and adjusted to a final volume of 12 mL with hexane. A 1.5-mL aliquot was centrifuged at 12,000 rpm for 10 min, and 1.2 mL of the supernatant was transferred to a GC vial for analysis.

GC-MS analysis was conducted on an Agilent 7890A-5975C system (Agilent Technologies, Santa Clara, CA, USA) equipped with a Varian CP7419 capillary column (0.25 μm, 50 m × 0.25 mm). Helium (purity ≥ 99.99%) was used as the carrier gas at a constant flow of 1.0 mL/min. The injector and detector temperatures were both set at 250°C. The mass spectrometer was operated in electron impact (EI) mode with a scan range of 50–550 amu. The injection volume was 1 μL. The oven temperature was initially held at 60°C for 0.5 min, increased to 155°C at 15°C/min, then to 175°C at 8°C/min, to 182°C at 1.2°C/min, and finally to 240°C at 15°C/min, with a post-run hold at 250°C for 2 min. Fatty acid methyl esters (FAMEs) were identified by comparison with the NIST11 mass spectral library and quantified using the C17:0 internal standard. Fatty acid content was expressed as mg per gram of dry cell weight (mg/g DCW).

2.7. Transcriptome analysis

Total RNA was extracted from liquid nitrogen-ground cells using TRIzol reagent with three biological replicates per condition. RNA concentration, purity, and integrity were evaluated using a NanoDrop 2000 spectrophotometer (Thermo Fisher Scientific, Waltham, MA, USA) and an Agilent 2100 Bioanalyzer (Agilent Technologies, Santa Clara, CA, USA). Only high-integrity RNA samples (RNA integrity number (RIN) ≥ 8.0, RNA concentration ≥ 50 ng/μL, total RNA > 1 μg, and $OD_{260}/_{280}$ ratio = 1.8–2.2) were used for library construction. Poly(A)+mRNA was enriched using oligo(dT)-coated magnetic beads, fragmented (~ 300 bp), and reverse-transcribed to construct cDNA libraries according to the standard Illumina protocol. Libraries were quantified using a QuantiFluor dsDNA System and sequenced on an Illumina HiSeq X Ten platform (Illumina, San Diego, CA, USA) to generate 150-bp paired-end reads.

Raw sequencing data were quality-checked with FastQC. High-quality reads were *de novo* assembled using Trinity, and transcript abundance was quantified using Salmon. Differential expression analysis was performed with DESeq2; genes with $|log_2(\text{fold change})| \geq 1$ and adjusted p-value < 0.01 were identified as significantly differentially expressed genes (DEGs). Functional annotation was conducted using Trinotate for Gene Ontology (GO) terms and BlastKOALA for KEGG Orthology assignment. GO and KEGG pathway enrichment analyses were performed with TBtools, and metabolic pathways were visualized using KEGG Mapper.

Global transcriptomic trends were explored via principal component analysis (PCA) on variance-stabilizing transformed counts. PCA, volcano plots (ggplot2), and hierarchical clustering heatmaps (pheatmap) were rendered using R version 4.5.3. Enrichment bar charts were prepared using Microsoft Excel 2019 (Microsoft Corporation, Redmond, WA, USA). The raw RNA-seq data have been deposited in the NCBI Sequence Read Archive (SRA) under accession number PRJNA1495189.

2.8. Statistical analysis

All experiments were conducted in biological triplicate, and data are presented as mean ± standard deviation (SD). One-way analysis of variance (ANOVA) followed by Tukey's HSD post-hoc test was used to evaluate the effects of glucose concentration, sea salt concentration, and initial pH on the yields of $\Delta^{5,7}$-sterols, astaxanthin, and DHA. PCA was performed to visualize overall variation and sample clustering based on the combined yields of the three target compounds. Permutational multivariate analysis of variance (PERMANOVA) with 999 permutations based on Euclidean distance was used to assess inter-group differences in multivariate product profiles. Statistical significance was set at $P < 0.05$. Statistical analyses were performed in R version 4.5.3 using the agricolae and vegan packages. Figures and illustrations were generated using Origin 2021 (OriginLab Corporation, Northampton, MA, USA), R, Microsoft Excel 2019, and Adobe Illustrator (Adobe Inc., San Jose, CA, USA).

3. Results and Discussion

3.1. The cell growth and changes of $\Delta^{5,7}$-sterols, astaxanthin and fatty acids of Schizochytrium sp. S31 under different concentrations of glucose

As shown in Fig. 1a, the DCW of *Schizochytrium* sp. S31 increased with the addition of glucose at 0–60 g/L, and nearly no residual glucose in culture medium, which demonstrated the glucose was mostly consumed by *Schizochytrium* sp. S31. The maximum DCW of 17.4 g/L was obtained at 60 g/L glucose concentration (Table 1). No significant different when glucose concentration increased from 60 to 90 g/L, but further addition of glucose (90–120 g/L) caused a slight decrease in DCW ($P < 0.05$), which may be due to high concentration of glucose causing hypertonic stress on the cells and inhibiting their growth (Guo et al., 2020), as further supported by microscopic observations showing decreased intracellular lipid droplets and a diminished granular appearance under high glucose concentrations (Figure S1). Nevertheless, the inhibition effect was not obvious within this range on *Schizochytrium* sp. S31. A comparably weak growth inhibition at high glucose levels has been reported for *Aurantiochytrium* sp. TC 20, a closely related strain within the family Thraustochytriidae, in which final biomass remained unchanged across initial glucose concentrations of 40–100 g/L (Lee Chang et al., 2013). The accumulation of residual glucose at initial glucose concentrations above 60 g/L indicated that glucose utilization efficiency of *Schizochytrium* sp. S31 decreased progressively with increasing glucose concentration (Fig. 1a).

Table 1

The yields of $\Delta^{5,7}$-sterols, astaxanthin, DHA and total fatty acids (TFAs) of *Schizochytrium* sp. S31 under different culture conditions.

Different conditions	$\Delta^{5,7}$-sterols (mg/L)	Astaxanthin (mg/L)	DHA (mg/L)	TFAs (mg/L)
Glucose Concentration (g/L)				
0	0.39 ± 0.13^{g}	0.08 ± 0.005^{d}	ND	ND
10	0.62 ± 0.02^{g}	0.61 ± 0.01^{b}	ND	ND
20	7.19 ± 0.27^{f}	0.76 ± 0.17^{a}	130.89 ± 6.84^{d}	303.33 ± 34.56^{d}
30	11.77 ± 0.46^{e}	0.49 ± 0.05^{b}	374.45 ± 8.57^{c}	2476.56 ± 46.65^{c}
40	14.45 ± 0.94^{d}	0.56 ± 0.12^{b}	673.22 ± 3.08^{b}	4140.77 ± 73.43^{b}
50	17.39 ± 0.51^{c}	0.60 ± 0.06^{b}	984.55 ± 85.38^{a}	6537.64 ± 67.45^{a}
60	21.26 ± 0.26^{a}	0.31 ± 0.05^{c}	974.42 ± 2.09^{a}	7068.59 ± 107.96^{a}
70	19.52 ± 0.38^{b}	0.30 ± 0.02^{c}	ND	ND
80	18.87 ± 0.03^{b}	0.30 ± 0.02^{c}	ND	ND
90	18.63 ± 0.12^{b}	0.25 ± 0.003^{c}	ND	ND
100	19.90 ± 0.08^{b}	0.26 ± 0.01^{c}	ND	ND
110	19.23 ± 0.44^{b}	0.24 ± 0.01^{c}	ND	ND
120	18.99 ± 0.37^{b}	0.22 ± 0.01^{c}	ND	ND
Sea salt Concentration (g/L)				
0	1.65 ± 0.03^{h}	0.33 ± 0.01^{a}	ND	ND
5	29.27 ± 0.49^{b}	0.11 ± 0.002^{b}	ND	ND
10	38.38 ± 0.05^{a}	0.07 ± 0.005^{c}	1141.19 ± 1.58^{a}	6498.41 ± 259.65^{a}
20	20.68 ± 0.91^{d}	0.36 ± 0.004^{a}	868.51 ± 19.33^{b}	6295.57 ± 246.01^{a}

*ND: Not detected.Values are mean ± SE. Different lowercase letters within the same column in each culture condition group indicate significant differences at $P < 0.05$ by one-way ANOVA followed by Duncan's multiple range test.

Different conditions	$\Delta^{5,7}$-sterols (mg/L)	Astaxanthin (mg/L)	DHA (mg/L)	TFAs (mg/L)
Glucose Concentration (g/L)				
30	21.77 ± 0.04^{c}	0.15 ± 0.03^{b}	620.73 ± 18.23^{c}	5307.19 ± 233.78^{b}
40	21.60 ± 1.42^{d}	0.11 ± 0.01^{b}	430.15 ± 37.74^{d}	3912.84 ± 203.08^{c}
50	20.55 ± 0.18^{d}	0.06 ± 0.0002^{c}	450.49 ± 18.72^{d}	4101.25 ± 211.31^{c}
60	19.33 ± 0.98^{d}	0.11 ± 0.02^{b}	ND	ND
70	18.88 ± 0.65^{d}	0.12 ± 0.01^{b}	ND	ND
80	20.23 ± 0.16^{d}	0.12 ± 0.002^{b}	ND	ND
90	15.40 ± 0.27^{e}	0.12 ± 0.004^{b}	ND	ND
110	14.33 ± 0.46^{f}	0.15 ± 0.01^{b}	ND	ND
130	11.27 ± 0.54^{g}	0.17 ± 0.005^{b}	ND	ND
pH				
3.5	4.92 ± 1.47^{d}	0.01 ± 0.002^{d}	1.96 ± 0.03^{c}	16.17 ± 0.19^{d}
4.5	$81.84 \pm 4..84^{a}$	0.02 ± 0.001^{d}	968.42 ± 8.15^{b}	5278.30 ± 161.57^{c}
5.5	50.73 ± 4.53^{b}	0.11 ± 0.02^{c}	1097.47 ± 8.06^{a}	6306.45 ± 6.93^{b}
6.5	37.95 ± 0.42^{c}	0.15 ± 0.01^{a}	1041.85 ± 47.78^{a}	6749.04 ± 74.50^{a}
7.5	36.39 ± 0.12^{c}	0.12 ± 0.003^{b}	957.77 ± 16.72^{b}	6836.79 ± 78.92^{a}

*ND: Not detected.Values are mean ± SE. Different lowercase letters within the same column in each culture condition group indicate significant differences at $P < 0.05$ by one-way ANOVA followed by Duncan's multiple range test.

Four $\Delta^{5,7}$-sterols, including ergosterol, C28-$\Delta^{5,7}$, C28-$\Delta^{5,7,24(28)}$ and C29-$\Delta^{5,7,22}$, were identified and determined in *Schizochytrium* sp. S31 in this work. Glucose concentration had no significant effect on the proportional composition of the four $\Delta^{5,7}$-sterols (Fig. 1b). In the canonical yeast ergosterol biosynthetic pathway, the C-22 desaturase ERG5 first converts C28-$\Delta^{5,7,24(28)}$ to ergosta-$\Delta^{5,7,22,24(28)}$-tetraen-3β-ol (C28-$\Delta^{5,7,22,24(28)}$), which is subsequently reduced by ERG4 at the C-24(28) double bond to

yield ergosterol (Ma et al., 2018). However, in our previous and current analysis using a modified UPLC-PDA method failed to detect the tetraene intermediate C28-$\Delta^{5,7,22,24(28)}$ at any growth stage of *Schizochytrium* sp. S31. Instead, C28-$\Delta^{5,7}$ and C29-$\Delta^{5,7,22}$ accumulated as the predominant products (Fig. 1b). These observations strongly suggest that *Schizochytrium* sp. S31 utilizes an alternative ergosterol biosynthetic route that differs from the canonical yeast pathway. In this proposed pathway, C28-$\Delta^{5,7,24(28)}$ undergoes direct C-24(28) reduction by ERG4 to form C28-$\Delta^{5,7}$, which is subsequently desaturated at C-22 by ERG5 to generate ergosterol. Concurrently, a portion of C28-$\Delta^{5,7,24(28)}$ enters the C29 branching pathway via a second methylation catalyzed by the bifunctional sterol C24-methyltransferase (24-SMT), ultimately yielding C29-$\Delta^{5,7,22}$. This distribution pattern likely arises from the low native expression and weak enzymatic activity of ERG5 in *Schizochytrium* sp. S31, leading to a substantial accumulation of its substrate (C28-$\Delta^{5,7}$) due to inefficient conversion to ergosterol. In contrast, C28-$\Delta^{5,7,24(28)}$ remains at the lowest level throughout the process, presumably because it is rapidly and competitively consumed by ERG4 and 24-SMT immediately upon formation. Notably, this alternative ergosterol biosynthetic pathway that bypasses the C28-$\Delta^{5,7,22,24(28)}$ intermediate is not unique to *Schizochytrium*; parallel pathways have been documented in the free-living protozoan *Acanthamoeba* (Zhou et al., 2018) and in parasitic kinetoplastid *Trypanosoma cruzi* (Urbina et al., 1995). Nonetheless, these hypotheses remain to be further validated by integrating comparative genomics analyses and isotope-tracing experiments.

At 20 g/L glucose, C28-$\Delta^{5,7}$ (0.92 mg/g DCW), C29-$\Delta^{5,7,22}$ (0.42 mg/g DCW), and C28-$\Delta^{5,7,24(28)}$ (0.053 mg/g DCW) reached their peaks, while ergosterol peaked at 0.32 mg/g DCW under 60 g/L glucose. Within the glucose concentration range of 0–50 g/L, the contents of all four $\Delta^{5,7}$-sterols initially increased and subsequently decreased. Interestingly, at glucose concentrations exceeding 50 g/L, the other three sterols exhibited a fluctuation trend opposite to that of C28-$\Delta^{5,7}$. This inverse relationship further indicates that C28-$\Delta^{5,7,24(28)}$ may act as a pivotal branch point in this strain. The multi-stage fluctuation, rather than a single shift, likely reflects the combined effects of changing carbon supply and increasing osmolarity at high glucose levels. This pattern aligns with the non-monotonic sterol response to osmotic stress reported in yeast (Mannazzu et al., 2008). Although the individual $\Delta^{5,7}$-sterol content per unit biomass fluctuated, the total volumetric production increased continuously from 0 to 60 g/L, reaching a maximum of 21.26 mg/L at 60 g/L of glucose concentration, and remained relatively stable thereafter (Table 1).

The carotenoids synthesized by *Schizochytrium* sp. S31 are mainly astaxanthin (Jiang et al., 2020). Astaxanthin, as a potent antioxidant, can effectively quench intracellular reactive oxygen species, thereby protecting cells against external environmental stress (Flores-Cotera et al., 2021). Under environmental stress, many microorganisms, such as *Phaffia rhodozyma*, can enhance astaxanthin synthesis and accumulation. Salinity stress has been demonstrated to trigger astaxanthin biosynthesis and increase cellular astaxanthin content in *Haematococcus pluvialis* (Kobayashi et al., 1997). In current study, the highest astaxanthin content (0.28 mg/g DCW) and yield (0.76 mg/L) were observed at 10 g/L glucose,

after which it declined and remained low with further increases in glucose concentration (Fig. 1c; Table 1).

In contrast, as the glucose concentration increased from 0 to 60 g/L, the TFA content rose continuously and peaked at 41.60% at 60 g/L (Fig. 1d). Meanwhile, DHA content initially increased and then plateaued, reaching a maximum of 6.02% DCW at 50 g/L. The yields of TFA and DHA followed similar trends, attaining maximums of 7069 mg/L and 985 mg/L, respectively. Given that blocking the terpenoid pathway by norflurazon can redirect carbon flux toward fatty acids in *Schizochytrium* sp. S31 (Bi et al., 2023), high glucose availability may similarly shift the metabolic flux allocation, prioritizing fatty acid synthesis over astaxanthin accumulation. Notably, the fatty acid profile exhibited a concentration-dependent shift across the glucose gradient (Table 2). At 20 g/L glucose, total unsaturated fatty acids (TUFAs) accounted for 64.46% of TFA, with DHA alone representing 43.20%. When glucose concentration was raised to 60 g/L, the proportion of TUFAs declined while that of saturated fatty acids (SFAs) increased. Consistent with this observation, elevated glucose concentrations in *Schizochytrium limacinum* SR21 favored SFA production rather than further enhancing DHA accumulation (Patel et al., 2020).

Table 2
Fatty acids profile of *Schizochytrium* sp. S31 at different glucose concentrations.

Fatty acids	Content (%TFAs)				
	20 g/L glucose	30 g/L glucose	40 g/L glucose	50 g/L glucose	60 g/L glucose
C12:0	ND	0.46 ± 0.11^{a}	0.45 ± 0.04^{a}	0.58 ± 0.08^{a}	0.60 ± 0.03^{a}
C13:0	ND	0.70 ± 0.12^{a}	0.37 ± 0.08^{b}	0.44 ± 0.01^{b}	0.40 ± 0.02^{b}
C14:0	3.16 ± 1.05^{c}	22.72 ± 0.07^{b}	22.47 ± 1.85^{b}	24.93 ± 1.12^{b}	26.35 ± 0.51^{a}
C15:0	3.03 ± 0.88^{c}	10.62 ± 1.21^{a}	7.20 ± 0.96^{b}	6.66 ± 0.33^{b}	6.34 ± 0.05^{b}
C16:0	29.37 ± 4.73^{b}	37.83 ± 0.37^{a}	37.35 ± 3.44^{a}	35.38 ± 0.08^{b}	33.63 ± 0.08^{b}
C16:1	0.93 ± 0.00^{e}	4.65 ± 0.04^{d}	7.24 ± 0.87^{c}	8.64 ± 0.20^{b}	10.51 ± 0.56^{a}
C18:0	0.44 ± 0.01^{b}	0.76 ± 0.11^{a}	0.68 ± 0.07^{a}	0.61 ± 0.003^{b}	0.52 ± 0.07^{b}
C18:1	0.48 ± 0.04^{d}	2.00 ± 0.04^{c}	2.17 ± 0.14^{c}	2.96 ± 0.004^{b}	3.77 ± 0.12^{a}
C20:4	ND	0.21 ± 0.01^{a}	0.18 ± 0.01^{b}	0.17 ± 0.01^{b}	0.14 ± 0.001^{c}
C20:5	19.85 ± 0.16^{a}	4.92 ± 0.11^{b}	5.25 ± 0.06^{b}	4.60 ± 0.37^{c}	3.96 ± 0.10^{d}
C22:6	43.20 ± 0.70^{a}	15.12 ± 0.41^{b}	16.65 ± 0.04^{b}	15.05 ± 1.10^{b}	13.79 ± 0.02^{c}
TUFAs	64.46 ± 0.90^{a}	26.91 ± 0.61^{c}	31.48 ± 1.12^{b}	31.41 ± 1.67^{b}	32.16 ± 0.81^{b}

*ND: Not detected. Data are presented as means ± SD ($n = 3$). Different lowercase letters denote significant differences at $p < 0.05$, as determined by one-way ANOVA followed by Tukey's HSD test.

TUFAs: total unsaturated fatty acids.

3.2. The cell growth and changes of $\Delta^{5,7}$-sterols, astaxanthin and fatty acids of Schizochytrium sp. S31 under different concentrations of sea salt

Schizochytrium sp. S31 failed to grow normally at 0 g/L sea salt and the DCW was only 0.66 g/L, indicating that *Schizochytrium* sp. S31 could not adapt to salt-free environment (Fig. 2a). The DCW increased with initial sea salt concentration from 0 to 20 g/L, reaching a maximum of 16.75 g/L; no significant difference in biomass was observed when the concentration was further increased to 30 g/L ($P > 0.05$). However, within the range of 30–80 g/L sea salt, the DCW declined gradually, followed by a more pronounced reduction from 90 to 130 g/L ($P < 0.05$). These growth dynamics aligned with microscopic observations across the salinity gradient: at 40–80 g/L sea salt, cells maintained uniform, spherical lipid droplets that progressively decreased in both size and abundance as salinity rose. At 90 g/L, lipid droplets dropped markedly, accompanied by plasmolysis in a subset of cells. By 110 g/L, lipid

droplets had nearly vanished, and at an extreme salinity of 130 g/L, no lipid droplets remained—yielding a homogeneous cytoplasm alongside cell wall thickening in certain *Schizochytrium* sp. S31 cells (Figure S2). The profiles of residual glucose across the sea salt gradient were basically consistent with the biomass trends, collectively indicating that high salinity suppressed both cell growth and substrate utilization (Ye et al., 2025).

Previous studies have reported varying salt tolerances among *Schizochytrium*; for instance, Yokochi et al. (1998) found that *Schizochytrium limacinum* SR21 exhibits robust halotolerance with an optimal growth salinity ranging from 50% to 200% of seawater (equivalent to 17.5–70.0 g/L sea salt); while Sun et al. (2018) reported that *Schizochytrium* sp. HX-308 achieved maximum biomass at 30 g/L. Notably, when the sea salt concentration increased to 130 g/L in the present study, growth was maintained and a DCW of 4.52 g/L was achieved, suggesting that *Schizochytrium* sp. S31 possesses a remarkable capacity to tolerate a wide range of salinity fluctuations.

Unlike the effect of glucose concentration, sea salt concentration significantly influenced both the contents and proportional compositions of the four $\Delta^{5,7}$-sterols. Low salinity (0–10 g/L) and high salinity (130 g/L) exerted pronounced effects, with a particularly sharp variation observed between 10 g/L and 20 g/L sea salt concentrations (Fig. 2). At low salinity, ergosterol predominated and peaked at 5 g/L (1.41 mg/g DCW), while C28-$\Delta^{5,7,24(28)}$ followed this trend, reaching 0.33 mg/g DCW. Between 20 and 110 g/L sea salt, the levels of ergosterol, C28-$\Delta^{5,7,24(28)}$, and C29-$\Delta^{5,7,22}$ remained stable. Conversely, C28-$\Delta^{5,7}$ predominated from 20 to 130 g/L, displaying a fluctuating trend that decreased initially (0 to 10 g/L) but rose steadily thereafter. Coupled with the known stress-responsive role of C28-$\Delta^{5,7}$ (Jiang et al., 2020), this shift suggests *Schizochytrium* sp. S31 dynamically regulates osmotic resistance using ergosterol at relatively low salinities and C28-$\Delta^{5,7}$ under hyperosmotic stress. Similarly, *Epicoccum nigrum* upregulates 9(11)-dehydroergosterol when shifted from freshwater to seawater (Ahumada-Rudolph et al., 2014). The total $\Delta^{5,7}$-sterol yield peaked at 38.38 mg/L at 10 g/L sea salt, declining thereafter (Table 1). This discrepancy with the biomass peak (20 g/L) suggests that the enhanced yield was driven by elevated cellular sterol content rather than increased cell density.

Under hypo-osmotic conditions (0 g/L sea salt), *Schizochytrium* sp. S31 growth was severely inhibited; however, astaxanthin content reached up to 0.50 mg/g DCW, which was 6.6- to 57.4-fold higher than the contents observed at all other salinities (Fig. 2c). Conversely, due to the higher biomass, the highest astaxanthin yield (0.36 mg/L) was obtained at 20 g/L sea salt (Table 1). DHA and TFA contents peaked at 10 g/L sea salt (7.3% and 41.3% of DCW, respectively), followed by a steady decline up to 40 g/L and a negligible recovery at 50 g/L that remained below low-salinity levels. This trend was followed by their yields, which also reached their maximum at 10 g/L (1141 and 6498 mg/L, respectively; Table 1). Concurrently, fatty acid profiling revealed that increasing salinity suppressed DHA and other PUFA (e.g., C20:5) proportions, while elevating SFAs such as C12:0, C14:0, and C15:0 (Table 3). This shift suggests that *Schizochytrium* sp. S31 increases membrane fatty acid saturation to reduce membrane fluidity and permeability, thereby protecting itself from hyperosmotic stress. This adaptive strategy accords with the

consensus that *Schizochytrium limacinum* primarily modulates fatty acid unsaturation to preserve membrane lipid homeostasis under salinity fluctuations (Zhu et al., 2007).

Table 3
Fatty acids profile of *Schizochytrium* sp. S31 at different sea salt concentrations.

Fatty acids	Content (%TFAs)				
	10 g/L sea salt	20 g/L sea salt	30 g/L sea salt	40 g/L sea salt	50 g/L sea salt
C12:0	0.43 ± 0.01^{b}	0.56 ± 0.02^{b}	0.70 ± 0.08^{b}	0.91 ± 0.09^{a}	1.10 ± 0.22^{a}
C13:0	0.36 ± 0.13^{b}	0.37 ± 0.02^{b}	0.50 ± 0.001^{b}	0.47 ± 0.03^{b}	0.72 ± 0.03^{a}
C14:0	20.29 ± 1.75^{c}	25.67 ± 0.87^{b}	28.48 ± 2.37^{b}	31.43 ± 0.03^{a}	32.34 ± 0.51^{a}
C15:0	7.74 ± 0.47^{a}	6.88 ± 1.08^{a}	6.50 ± 0.57^{a}	7.14 ± 0.53^{a}	6.99 ± 0.17^{a}
C16:0	43.03 ± 1.29^{a}	37.71 ± 3.64^{b}	31.87 ± 0.58^{c}	28.56 ± 1.54^{c}	27.72 ± 0.08^{c}
C16:1	2.78 ± 0.34^{c}	7.78 ± 1.12^{b}	12.62 ± 0.26^{a}	13.05 ± 0.16^{a}	12.85 ± 0.67^{a}
C18:0	0.78 ± 0.03^{a}	0.57 ± 0.02^{b}	0.55 ± 0.003^{b}	0.45 ± 0.09^{b}	0.42 ± 0.04^{c}
C18:1	1.28 ± 0.20^{c}	2.48 ± 0.49^{b}	3.72 ± 0.24^{a}	3.97 ± 0.09^{a}	3.95 ± 0.07^{a}
C20:4	0.26 ± 0.02^{a}	0.17 ± 0.01^{b}	0.10 ± 0.01^{c}	0.11 ± 0.02^{c}	0.12 ± 0.01^{c}
C20:5	5.50 ± 0.05^{a}	4.01 ± 0.11^{b}	3.27 ± 0.11^{c}	2.92 ± 0.25^{c}	2.81 ± 0.01^{d}
C22:6	17.56 ± 0.09^{a}	13.79 ± 0.39^{b}	11.70 ± 0.36^{c}	10.99 ± 0.75^{c}	10.99 ± 0.04^{c}
TUFAs	27.37 ± 0.69^{b}	28.24 ± 2.13^{b}	31.40 ± 0.98^{a}	31.02 ± 1.27^{a}	30.72 ± 0.80^{b}

Data are presented as means ± SD ($n = 3$). Different lowercase letters denote significant differences at $p < 0.05$, as determined by one-way ANOVA followed by Tukey's HSD test.

TUFAs: total unsaturated fatty acids.

3.3. The cell growth and changes of $\Delta^{5,7}$-sterols, astaxanthin and fatty acids of Schizochytrium sp. S31 under different pH conditions

The effects of pH on *Schizochytrium* sp. S31 biomass and residual glucose are illustrated in Fig. 3a. At pH 3.5, cell growth was severely suppressed, yielding a minimal DCW of only 0.52 g/L alongside high residual glucose. This strong inhibition stems from the disruption of ion homeostasis; as established by Shabala et al. (2001), *Schizochytrium* proliferation depends on stable transmembrane H^+ and Na^+ fluxes. Consequently, excessive extracellular H^+ impairs both ionic balance and nutrient transport, ultimately arresting cell growth. Morphologically, cells cultured at pH 3.5 exhibited no distinct lipid droplets and

presented transparent intracellular vacuoles. At pH 4.5, although vacuoles persisted in a subset of cells, intracellular lipid droplets increased noticeably. By pH 5.5, vacuoles had largely disappeared, and further increases in initial pH promoted progressive expansion in both the abundance and diameter of intracellular lipid droplets (Figure S3). Concurrently, biomass increased with pH from 3.5 to 5.5, peaking at 16.40 g/L at pH 5.5, while glucose consumption profiles closely paralleled these growth dynamics. Notably, the stable growth observed within the pH 4.5–7.5 range indicates that strain S31 is relatively insensitive to pH variations under this regime. This wide adaptability aligns with reports by Zhao et al. (2017), who noted that *Schizochytrium* sp. AB-610 tolerates pH 4–8 with shorter lag phases near neutrality, as well as findings by Wu et al. (2005) where maximum biomass was achieved at pH 7. Literáková et al. (2024) identified a slightly lower optimum of pH 6.5 for *S. marinum* AN-4 and *S. limacinum* CO3H (tested range: pH 3.7–6.8). Conversely, Bouras et al. (2022) reported that *S. limacinum* SR21 achieved maximal biomass at pH 7.0 within a more alkaline testing range (pH 6.0–9.0).

Ergosterol and C28-$\Delta^{5,7}$ exhibited synchronous intracellular accumulation, maximizing at pH 3.5 and declining as pH rose (Fig. 3b). This trend likely reflects a membrane-stress adaptation; the acid stress at pH 3.5 prompted robust sterol synthesis to reinforce plasma membrane stability against acid-induced damage. This aligns with the general eukaryotic stress response, where microbial cells actively modulate sterol biosynthesis to preserve membrane integrity and protein function under environmental challenges (Guan et al., 2009). As acid stress alleviated at pH 4.5, biomass recovered while ergosterol and C28-$\Delta^{5,7}$ dropped sharply; meanwhile, C29-$\Delta^{5,7,22}$ and C28-$\Delta^{5,7,24(28)}$ reached their respective maxima (1.44 and 0.52 mg/g DCW). Within the pH 4.5–7.5, the four $\Delta^{5,7}$-sterols shifted synchronously, indicating constant compositional ratios despite a declining total sterol content, which drove a peak total yield of 81.84 mg/L at pH 4.5 (Table 1). Furthermore, the abundance order (ergosterol > C29-$\Delta^{5,7,22}$ > C28-$\Delta^{5,7}$ > C28-$\Delta^{5,7,24(28)}$) perfectly matched the baseline profile at 10 g/L sea salt in Section 3.2, confirming this pattern as an intrinsic characteristic of basal metabolism.

Figure 3c and Table 4 illustrate distinct pH-dependent metabolic patterns for astaxanthin and TFA in *Schizochytrium* sp. S31. Astaxanthin content peaked at pH 3.5 (0.016 mg/g DCW) but reached its minimal level at pH 4.5 (0.001 mg/g DCW), while its yield stabilized betweenpH 5.5 and 7.5 (peaking at pH 6.5, 0.15 mg/L). For fatty acids, TFA content and production rose continuously with pH, maximizing at 432.48 mg/g and 6836.79mg/L at pH 7.5, respectively. In contrast, DHA content and yield prioritized a slightly acidic optimum, maximizing at pH 5.5 (66.94 mg/g and 1097.47 mg/L). This preferential biosynthesis of DHA under moderate acidity aligns with previous studies; for instance, Yin et al. (2019) and Zhao et al. (2017) both enhanced DHA production in *Schizochytrium* by transitioning the pH from 7.0 during growth down to 5.0 during fatty acid synthesis, confirming that acidic shifts favor DHA biosynthesis. Crucially, the acidic stress at pH 3.5 severely impaired fatty acid accumulation, rendering C12:0 and C20:4 undetectable (Table 4), and reducing TFAs to approximately 9.1% of the level at pH 4.5.

Table 4
Fatty acids profile of *Schizochytrium* sp.S31 under different pH conditions.

Fatty acids	Content (%TFAs)				
	pH 3.5	pH 4.5	pH 5.5	pH 6.5	pH 7.5
C12:0	ND	0.47 ± 0.08^{b}	0.51 ± 0.01^{b}	0.62 ± 0.003^{a}	0.68 ± 0.003^{a}
C13:0	2.30 ± 0.27^{a}	0.61 ± 0.01^{b}	0.27 ± 0.01^{c}	0.29 ± 0.04^{b}	0.53 ± 0.01^{b}
C14:0	3.94 ± 0.25^{e}	18.69 ± 0.61^{d}	22.21 ± 0.20^{c}	25.04 ± 0.24^{b}	25.95 ± 0.19^{a}
C15:0	51.12 ± 1.25^{a}	12.08 ± 0.28^{b}	5.68 ± 0.39^{d}	5.49 ± 0.04^{d}	7.14 ± 0.08^{c}
C16:0	19.26 ± 0.50^{d}	41.22 ± 1.36^{a}	38.96 ± 0.19^{b}	34.32 ± 0.68^{c}	32.50 ± 0.54^{c}
C16:1	1.94 ± 0.28^{c}	0.96 ± 0.05^{d}	5.81 ± 0.31^{b}	9.88 ± 0.53^{a}	10.63 ± 0.06^{a}
C18:0	1.03 ± 0.12^{a}	0.77 ± 0.03^{b}	0.71 ± 0.01^{b}	0.60 ± 0.04^{c}	0.54 ± 0.01^{c}
C18:1	4.42 ± 0.06^{a}	0.63 ± 0.01^{d}	2.76 ± 0.02^{c}	3.43 ± 0.20^{b}	3.58 ± 0.02^{b}
C20:4	ND	0.22 ± 0.01^{a}	0.20 ± 0.002^{a}	0.17 ± 0.005^{a}	0.16 ± 0.11^{a}
C20:5	2.87 ± 0.08^{e}	6.00 ± 0.04^{a}	5.48 ± 0.11^{b}	4.74 ± 0.22^{c}	4.28 ± 0.11^{d}
C22:6	12.12 ± 0.24^{e}	18.35 ± 0.06^{a}	17.40 ± 0.26^{b}	15.44 ± 0.64^{c}	14.01 ± 0.20^{d}
TUFAs	21.35 ± 0.66^{c}	26.16 ± 0.17^{b}	31.66 ± 0.71^{a}	33.65 ± 1.60^{a}	32.66 ± 0.40^{a}

*ND: Not detected. Data are presented as means ± SD ($n = 3$). Different lowercase letters denote significant differences at $p < 0.05$, as determined by one-way ANOVA followed by Tukey's HSD test.

TUFAs: total unsaturated fatty acids.

3.4 Multivariate evaluation and single-factor optimization for co-production in Schizochytrium sp. S31

PCA showed that the first two principal components explained 55.3% and 32.8% of the total variance, respectively, cumulatively accounting for 88.1% of the total variation in the yields of $\Delta^{5,7}$-sterols, astaxanthin and DHA of *Schizochytrium* sp. S31 across glucose, sea salt and pH gradient treatments (Fig. 4a). PERMANOVA further confirmed statistically significant differences in product yield profiles among the three treatment groups ($R^2 = 0.207$, $P = 0.002$), which was consistent with the partially separated clustering patterns and 95% confidence ellipses observed in the ordination plot. The separation along the PC1 axis was primarily driven by DHA and $\Delta^{5,7}$-sterols, whereas astaxanthin represented the main source of variance along PC2, as indicated by the length and direction of their respective loading vectors. Specifically, pH treatments favored DHA and $\Delta^{5,7}$-sterol yields, glucose

treatments shifted toward higher astaxanthin accumulation, and sea salt treatments occupied an intermediate position without marked bias. Regarding inter-variable associations, the small acute angle between DHA and $\Delta^{5,7}$-sterol loading vectors indicated a strong positive co-yield correlation, whereas astaxanthin diverged, reflecting decoupled synthesis. Analysis of sample scores further revealed that samples cultured under 60 g/L glucose, 10 g/L sea salt and pH 5.5 were positioned at the outer edges of their respective confidence ellipse, pointing directly toward the direction of the dominant product vectors. These spatial locations within the ordination plot demonstrate that these specific parameter levels achieved the highest comprehensive product yields within each single-factor gradient.

The growth curve of *Schizochytrium* sp. S31 under the optimal culture conditions is shown in Fig. 4b, with the biomass reaching its maximum on Day 6 of cultivation. At this time point, the total $\Delta^{5,7}$-sterol, DHA, and astaxanthin yields reached 50.73, 1097.47, and 0.11 mg/L, respectively. However, since these findings were derived from independent single-factor experiments, and the interactive effects among glucose concentration, sea salt concentration, and pH remain to be elucidated. Multi-factor optimization experiments are therefore required to further enhance the co-production process of these three high-value products.

3.5 Transcriptomic regulation of sterol, carotenoid, and fatty acid biosynthesis in Schizochytrium sp. S31

Single-factor experiments identified sea salt concentration as the primary factor influencing the accumulation of sterols, astaxanthin, and fatty acids in *Schizochytrium* sp. S31. Compared with the 20 g/L control, 10 g/L sea salt significantly reshaped the $\Delta^{5,7}$-sterols profile and enhanced total yields of $\Delta^{5,7}$-sterols, DHA, and total fatty acids, while decreasing astaxanthin yield. Transcriptomic analysis was subsequently performed to uncover the underlying pathways modulating this divergent accumulation pattern. Clear transcriptomic divergence was observed between the two groups (Fig. 5a–c), with DEGs heavily enriched in key lipid metabolic networks, specifically fatty acid biosynthesis/degradation, sterol biosynthesis, and carotenoid biosynthesis (Fig. 5d–e; Table S4).

To elucidate the molecular mechanisms underlying sea salt-regulated multi-product biosynthesis, central metabolic pathways of *Schizochytrium* sp. S31 were reconstructed using KEGG Mapper, mapping DEGs onto specific enzymatic nodes (Fig. 6). At the glycolytic node, differential gene expression directly tuned acetyl-CoA precursor supply: *ENO* and *gpmB* were upregulated, whereas *GAPDH* and *PK* were downregulated, alongside divergent expression of pyruvate dehydrogenase components (*aceE* upregulated; *PDHA* downregulated). As acetyl-CoA enters the mevalonate (MVA) pathway to supply terpenoid precursors (IPP and DMAPP), upstream *HMGCS* was upregulated 2.95-fold, favoring precursor generation for both sterol and carotenoid synthesis. Within the sterol branch, *FDFT1* and *ERG11* were downregulated 2.0- and 2.95-fold, respectively, whereas the downstream Δ^{14}-sterol reductase gene *ERG24* was upregulated 2.46-fold. This transcriptional downregulation of key upstream sterol genes at the late growth phase likely reflects negative feedback regulation following the substantial intracellular accumulation of sterols, while the differential expression of downstream reductases and desaturases

rationalizes the reshaped sterol compositional profile. Additionally, transcriptomic analysis revealed the expression of key genes involved in the biosynthesis pathways of cholesterol, campesterol, brassicasterol, and stigmasterol (Fig. S4), suggesting that *Schizochytrium* sp. S31 possesses the functional potential to synthesize these four sterols.

Concurrently, carbon allocation toward the carotenoid pathway was reinforced by the upregulation of *GGPS1* and *crtB*, driving massive phytoene accumulation (Wan et al., 2021). However, downstream crtI and crtR were downregulated 2.65- and 2.33-fold, respectively, directly accounting for the reduced astaxanthin content. Regarding fatty acid metabolism, *ACACA* was downregulated 6.28-fold, while elongation and desaturation genes exhibited mixed responses (*fabF*, *fabG*, and *ELOVL5* upregulated; *fabL*, *fabZ*, and *FADS2* downregulated). Crucially, key fatty acid β-oxidation genes—including *ACOX1* (upregulated 7.21- to 17.39-fold), *fadA*, *fadN*, *echA*, and *ACAT*—were markedly upregulated. This enhanced β-oxidation under late-stage carbon depletion provided energy while generating supplementary acetyl-CoA to feed the MVA pathway. Furthermore, the preferential degradation of short-chain fatty acids over polyunsaturates helps explain the elevated DHA proportion observed under low sea salt condition (Chang et al., 2013). The current approach was insufficient to elucidate whether a polyketide synthase (PKS) pathway exists in *Schizochytrium* sp. S31 and how it interacts with the fatty acid synthase (FAS) pathway. Future studies utilizing whole-genome sequencing and RT-PCR are warranted to verify the presence of PKS-related genes, alongside gene knockout, RNA interference, or enzyme inhibition techniques to clarify the role of the PKS pathway in fatty acid synthesis, as well as to experimentally validate the metabolic crosstalk among the biosynthesis pathways of sterols, DHA, and astaxanthin.

4. Conclusion

The growth characteristics and the changes of sterols, astaxanthin and fatty acids in *Schizochytrium* sp. S31 were investigated in this study. At an initial glucose concentration of 60 g/L, *Schizochytrium* sp. S31 achieved a maximum biomass of 17.4 g/L. Across all tested glucose levels, the abundance order of the four $\Delta^{5,7}$-sterols remained consistent: C28-$\Delta^{5,7}$ > C29-$\Delta^{5,7,22}$ > ergosterol > C28-$\Delta^{5,7,24(28)}$. Below 60 g/L glucose, the contents of TFA and DHA increased with rising glucose concentration, whereas astaxanthin content exhibited a slight decline. Glucose concentrations exceeding 60 g/L exerted minimal impacts on both biomass and astaxanthin accumulation. Cell growth of *Schizochytrium* sp. S31 was noticeably suppressed at sea salt concentrations below 10 g/L or above 80 g/L. At 10 g/L sea salt, the total $\Delta^{5,7}$-sterol content peaked at approximately 2 mg/g DCW, with ergosterol constituting the largest proportion (41%). Concurrently, TFA and DHA contents reached their highest levels at 41.3% and 7.3% DCW, respectively. At salinities exceeding 10 g/L, C28-$\Delta^{5,7}$ became the predominant $\Delta^{5,7}$-sterol; meanwhile, DHA and TFA contents gradually declined, whereas astaxanthin content exhibited an upward trend. Regarding initial pH, cell proliferation was severely inhibited at pH 3.5, while maximal biomass was attained at pH 5.5. Within the pH range of 5.5–7.5, biomass, total $\Delta^{5,7}$-sterol content, and the contents of DHA and astaxanthin remained relatively stable.

Single-factor evaluations demonstrated that a culture medium containing 60 g/L glucose, 10 g/L sea salt, and an initial pH of 5.5 supported optimal cell growth. Under these conditions, *Schizochytrium* sp. S31 efficiently co-accumulated sterols, DHA, and astaxanthin, achieving maximal volumetric yields of 50.73 mg/L for total $\Delta^{5,7}$-sterols and 1097.47 mg/L for DHA, alongside an astaxanthin yield of 0.11 mg/L. Transcriptomic analysis further revealed tight metabolic coordination among the biosynthesis pathways of sterols, DHA, and astaxanthin under low-salinity conditions. Enhanced fatty acid β-oxidation promoted the precursor supply of acetyl-CoA toward the MVA pathway, thereby modulating downstream sterol and carotenoid synthesis. Specifically, astaxanthin accumulation was down-regulated through the transcriptional repression of crtI and crtR. Additionally, transcriptomic data confirmed the active transcription of candidate genes involved in the biosynthesis of cholesterol, campesterol, brassicasterol, and stigmasterol in *Schizochytrium* sp. S31.

Overall, these findings not only broaden the understanding of the physiological responses of *Schizochytrium* sp. S31 under varying culture conditions, but also provide crucial insights and a promising strategy for the co-production of multi-value bioactives in thraustochytrid cell factories.

Declarations

Author Contribution

Xiao-Yu Zhang and Pei-Shan He: Methodology, Data curation, Writing-original draft. Yi-Nan Liao: Methodology, Resources. Juan Peng: Supervision, Conceptualization, Investigation, Visualization, Data curation. Jian-Ping Yuan: Writing- review&editing. Jun Zhao: Project administration, Writing-review & editing.

Acknowledgements

This work was supported by the Research Project of Southern Marine Science and Engineering Guangdong Laboratory (Zhuhai), Guangdong Province, China (SML2024SP029), the Key Technologies Research and Development Program of Guangzhou, Guangdong Province, China (2023B03J1379), and the Fund of the National Science Foundation of Guangdong Province, China (2021A1515012589).

References

1. Jiang YL, Zhu Q, Liao YN, Wang QQ, Li Y, Dong XY, Peng J, Yuan JP, Wang JH (2020) The delta 5, 7-sterols and astaxanthin in the marine microheterotroph *Schizochytrium* sp. S31. J Am Oil Chem Soc 97:839–850. https://doi.org/10.1002/aocs.12364
2. Kalidasan K, Vinithkumar NV, Peter DM, Dharani G, Dufossé L (2021) Thraustochytrids of mangrove habitats from andaman islands: species diversity, PUFA profiles and biotechnological potential. Mar Drugs 19:571. https://doi.org/10.3390/md19100571

3. Lee KJ, Chang GA, Dunstan GCJ, Abell LA, Clementson SI, Blackburn PD, Nichols A, Koutoulis (2012) Biodiscovery of new australian thraustochytrids for production of biodiesel and long-chain omega-3 oils. Appl Microbiol Biotechnol 93:2215–2231. https://doi.org/10.1007/s00253-011-3856-4
4. Bochdansky AB, Clouse MA, Herndl GJ (2017) Eukaryotic microbes, principally fungi and labyrinthulomycetes, dominate biomass on bathypelagic marine snow. ISME J 11:362–373. https://doi.org/10.1038/ismej.2016.113
5. Song Y, Yang X, Li S, Luo Y, Chang JS, Hu Z (2024) Thraustochytrids as a promising source of fatty acids, carotenoids, and sterols: bioactive compound biosynthesis, and modern biotechnology. Crit Rev Biotechnol 44:618–640. https://doi.org/10.1080/07388551.2023.2196373
6. Peng Z, Zhong L, Li Y, Feng S, Mou J, Miao Y, Lin CSK, Wang Z, Li X (2025) Harnessing oleaginous protist *Schizochytrium* for docosahexaenoic acid: current technologies in sustainable production and food applications. Food Res Int 205:115996. https://doi.org/10.1016/j.foodres.2025.115996
7. Xie S, Wei D, Tan B, Liu Y, Tian L, Niu J (2020) *Schizochytrium limacinum* supplementation in a low fish-meal diet improved immune response and intestinal health of juvenile *Penaeus monodon*. Front Physiol 11:613. https://doi.org/10.3389/fphys.2020.00613
8. Shi Y, Cao X, Ye Z, Xu Y, Wang Y, Li Z, Hang W, He N (2021) Role of dietary *Schizochytrium* sp. in improving disease resistance of zebrafish through metabolic and microbial analysis. Aquaculture 539:736631. https://doi.org/10.1016/j.aquaculture.2021.736631
9. Chi G, Xu Y, Cao X, Li Z, Cao M, Chisti Y, He N (2022) Production of polyunsaturated fatty acids by *Schizochytrium* (*Aurantiochytrium*) spp., Biotechnol. Adv 55:107897. https://doi.org/10.1016/j.biotechadv.2021.107897
10. Permanasari SWA, Lin HC, Lin JY, Hong MX, Chang HY, He WD, Lo LH, Yang YL, Lee TM, Liaw CC (2026) MALDI-TOF MS classification of formosan thraustochytrids and their use in shrimp farming. J Agric Food Chem 74:10747–10758. https://doi.org/10.1021/acs.jafc.5c08939
11. Ramos-Vega A, Rosales-Mendoza S, Bañuelos-Hernández B, Angulo C (2018) Prospects on the use of *Schizochytrium* sp. to develop oral vaccines. Front Microbiol 9:2506. https://doi.org/10.3389/fmicb.2018.02506
12. Ganuza E, Anderson AJ, Ratledge C (2008) High-cell-density cultivation of *Schizochytrium* sp. in an ammonium/pH-auxostat fed-batch system. Biotechnol Lett 30:1559–1564. https://doi.org/10.1007/s10529-008-9723-4
13. Wu ST, Lin LP (2003) Application of response surface methodology to optimize docosahexaenoic acid production by *Schizochytrium* sp. s31. J Food Biochem 27:127–139. https://doi.org/10.1111/j.1745-4514.2003.tb00271.x
14. Ye S, Wang X, Zhou Y, Xiao X, Liu P, Chi C, Sun P, Zheng M, Chen B, Mao R, He Y (2025) Effects of salinity on the growth performance and docosahexaenoic acid positional distribution in triacylglycerols of the newly isolated *Schizochytrium* sp. FJ-1, Mar. Drugs 23 260. https://doi.org/10.3390/md23070260

15. Zhu L, Zhang X, Ji L, Song X, Kuang C (2007) Changes of lipid content and fatty acid composition of *Schizochytrium limacinum* in response to different temperatures and salinities. Process Biochem 42:210–214. https://doi.org/10.1016/j.procbio.2006.08.002
16. Zhao B, Li Y, Mbifile MD, Li C, Yang H, Wang W (2017) Improvement of docosahexaenoic acid fermentation from *Schizochytrium* sp. AB-610 by staged pH control based on cell morphological changes. Eng Life Sci 17:981–988. https://doi.org/10.1002/elsc.201600249
17. Da Costa JCCS, Guimarães LA, Da Luz A, De Freitas LP, De Souza Vandenberghe GV, De Melo Pereira CR, Soccol HLG, Rogez (2026) Insights from meta-analysis for efficient docosahexaenoic acid production in thraustochytrids through advanced cultivation and fermentation strategies. Biofuels Bioprod Biorefin 20:1041–1060. https://doi.org/10.1002/bbb.70100
18. Caspeta L, Chen Y, Ghiaci P, Feizi A, Buskov S, Hallström BM, Petranovic D, Nielsen J (2014) Altered sterol composition renders yeast thermotolerant. Science 346:75–78. https://doi.org/10.1126/science.1258137
19. Dupont S, Beney L, Ferreira T, Gervais P (2011) Nature of sterols affects plasma membrane behavior and yeast survival during dehydration, Biochim. Biophys. Acta (BBA) - Biomembr. 1808:1520–1528. https://doi.org/10.1016/j.bbamem.2010.11.012
20. Miller GL (1959) Use of dinitrosalicylic acid reagent for determination of reducing sugar. Anal Chem 31:426–428. https://doi.org/10.1021/ac60147a030
21. Koopmann IK, Müller BA, Labes A (2023) Screening of a thraustochytrid strain collection for carotenoid and squalene production characterized by cluster analysis, comparison of 18S rRNA gene sequences, growth behavior, and morphology. Mar Drugs 21:204. https://doi.org/10.3390/md21040204
22. Zhang CW, Zhang FL, Dong SJ, He YY, Xu XM, Peng J, Yuan JP (2019) The discrepancy of fatty acid composition of astaxanthin esters and total fatty acids in photoautotrophic and heterotrophic *Chlorella zofingiensis*. J Am Oil Chem Soc 96:891–901. https://doi.org/10.1002/aocs.12230
23. Guo DS, Tong LL, Ji XJ, Ren LJ, Ding QQ (2020) Development of a strategy to improve the stability of culture environment for docosahexaenoic acid fermentation by *Schizochytrium* sp. Appl Biochem Biotechnol 192:881–894. https://doi.org/10.1007/s12010-020-03298-7
24. Lee Chang KJ, Dumsday G, Nichols PD, Dunstan GA, Blackburn SI, Koutoulis A (2013) High cell density cultivation of a novel *Aurantiochytrium* sp. strain tc 20 in a fed-batch system using glycerol to produce feedstock for biodiesel and omega-3 oils. Appl Microbiol Biotechnol 97:6907–6918. https://doi.org/10.1007/s00253-013-4965-z
25. Ma BX, Ke X, Tang XL, Zheng RC, Zheng YG (2018) Rate-limiting steps in the *Saccharomyces cerevisiae* ergosterol pathway: towards improved ergosta-5,7-dien-3β-ol accumulation by metabolic engineering. World J Microbiol Biotechnol 34:55. https://doi.org/10.1007/s11274-018-2440-9
26. Zhou W, Warrilow AGS, Thomas CD, Ramos E, Parker JE, Price CL, Vanderloop BH, Fisher PM, Loftis MD, Kelly DE, Kelly SL, Nes WD (2018) Functional importance for developmental regulation of sterol

biosynthesis in *Acanthamoeba castellanii*, Biochim. Biophys. Acta (BBA) - Mol. Cell Biol Lipids 1863:1164–1178. https://doi.org/10.1016/j.bbalip.2018.07.004

27. Urbina JA, Vivas J, Visbal G, Contreras LM (1995) Modification of the sterol composition of *Trypanosoma (Schizotrypanum) cruzi* epimastigotes by Δ24(25)-sterol methyl transferase inhibitors and their combinations with ketoconazole. Mol Biochem Parasitol 73:199–210. https://doi.org/10.1016/0166-6851(95)00117-J
28. Mannazzu I, Angelozzi D, Belviso S, Budroni M, Farris GA, Goffrini P, Lodi T, Marzona M, Bardi L (2008) Behaviour of *Saccharomyces cerevisiae* wine strains during adaptation to unfavourable conditions of fermentation on synthetic medium: cell lipid composition, membrane integrity, viability and fermentative activity. Int J Food Microbiol 121:84–91. https://doi.org/10.1016/j.ijfoodmicro.2007.11.003
29. Flores-Cotera LB, Chávez-Cabrera C, Martínez-Cárdenas A, Sánchez S, García-Flores OU (2021) Deciphering the mechanism by which the yeast *Phaffia rhodozyma* responds adaptively to environmental, nutritional, and genetic cues. J Ind Microbiol Biotechnol 48:kuab048. https://doi.org/10.1093/jimb/kuab048
30. Kobayashi M, Kurimura Y, Tsuji Y (1997) Light-independent, astaxanthin production by the green microalga *Haematococcus pluvialis* under salt stress. Biotechnol Lett 19:507–509. https://doi.org/10.1023/A:1018372900649
31. Bi Y, Guo P, Liu L, Chen L, Zhang W (2023) Elucidation of sterol biosynthesis pathway and its co-regulation with fatty acid biosynthesis in the oleaginous marine protist *Schizochytrium* sp. Front Bioeng Biotechnol 11:1188461. https://doi.org/10.3389/fbioe.2023.1188461
32. Patel A, Liefeldt S, Rova U, Christakopoulos P, Matsakas L (2020) Co-production of DHA and squalene by thraustochytrid from forest biomass, Sci. Rep. 10 1992. https://doi.org/10.1038/s41598-020-58728-7
33. Yokochi T, Honda D, Higashihara T, Nakahara T (1998) Optimization of docosahexaenoic acid production by *Schizochytrium limacinum* SR21. Appl Microbiol Biotechnol 49:72–76. https://doi.org/10.1007/s002530051139
34. Sun XM, Ren LJ, Bi ZQ, Ji XJ, Zhao QY, Huang H (2018) Adaptive evolution of microalgae *Schizochytrium* sp. under high salinity stress to alleviate oxidative damage and improve lipid biosynthesis. Bioresour Technol 267:438–444. https://doi.org/10.1016/j.biortech.2018.07.079
35. Ahumada-Rudolph R, Cajas-Madriaga D, Rudolph A, Reinoso R, Torres C, Silva M, Becerra J (2014) Variation of sterols and fatty acids as an adaptive response to changes in temperature, salinity and pH of a marine fungus *Epicoccum nigrum* isolated from the patagonian fjords. Rev Biol Mar Oceanogr 49:293–305. https://doi.org/10.4067/S0718-19572014000200009
36. Shabala L, Shabala S, Ross T, McMeekin T (2001) Membrane transport activity and ultradian ion flux oscillations associated with cell cycle of *Thraustochytrium* sp. Aust J Plant Physiol 28:87–99. https://doi.org/10.1071/PP00121

37. Wu ST, Yu ST, Lin LP (2005) Effect of culture conditions on docosahexaenoic acid production by *Schizochytrium* sp. S31. Process Biochem 40:3103–3108. https://doi.org/10.1016/j.procbio.2005.03.007
38. Literáková P, Zavřel T, Búzová D, Kaštánek P, Červený J (2024) Marine microalgae *Schizochytrium* demonstrates strong production of essential fatty acids in various cultivation conditions, advancing dietary self-sufficiency. Front Nutr 11:1290701. https://doi.org/10.3389/fnut.2024.1290701
39. Bouras S, Antoniadis D, Kountrias G, Karapanagiotidis IT, Katsoulas N (2022) Effect of pH on *Schizochytrium limacinum* production grown using crude glycerol and biogas digestate effluent. Agronomy 12:364. https://doi.org/10.3390/agronomy12020364
40. Guan XL, Souza CM, Pichler H, Dewhurst G, Schaad O, Kajiwara K, Wakabayashi H, Ivanova T, Castillon GA, Piccolis M, Abe F, Loewith R, Funato K, Wenk MR, Riezman H (2009) Functional interactions between sphingolipids and sterols in biological membranes regulating cell physiology. Mol Biol Cell 20:2083–2095. https://doi.org/10.1091/mbc.e08-11-1126
41. Yin FW, Zhang YT, Jiang JY, Guo DS, Gao S, Gao Z (2019) Efficient docosahexaenoic acid production by *Schizochytrium* sp. via a two-phase pH control strategy using ammonia and citric acid as pH regulators. Process Biochem 77:1–7. https://doi.org/10.1016/j.procbio.2018.11.013
42. Wan X, Zhou XR, Moncalian G, Su L, Chen WC, Zhu HZ, Chen D, Gong YM, Huang FH, Deng QC (2021) Reprogramming microorganisms for the biosynthesis of astaxanthin via metabolic engineering, Prog. Lipid Res 81:101083. https://doi.org/10.1016/j.plipres.2020.101083
43. Chang G, Luo Z, Gu S, Wu Q, Chang M, Wang X (2013) Fatty acid shifts and metabolic activity changes of *Schizochytrium* sp. S31 cultured on glycerol. Bioresour Technol 142:255–260. https://doi.org/10.1016/j.biortech.2013.05.030

Figures

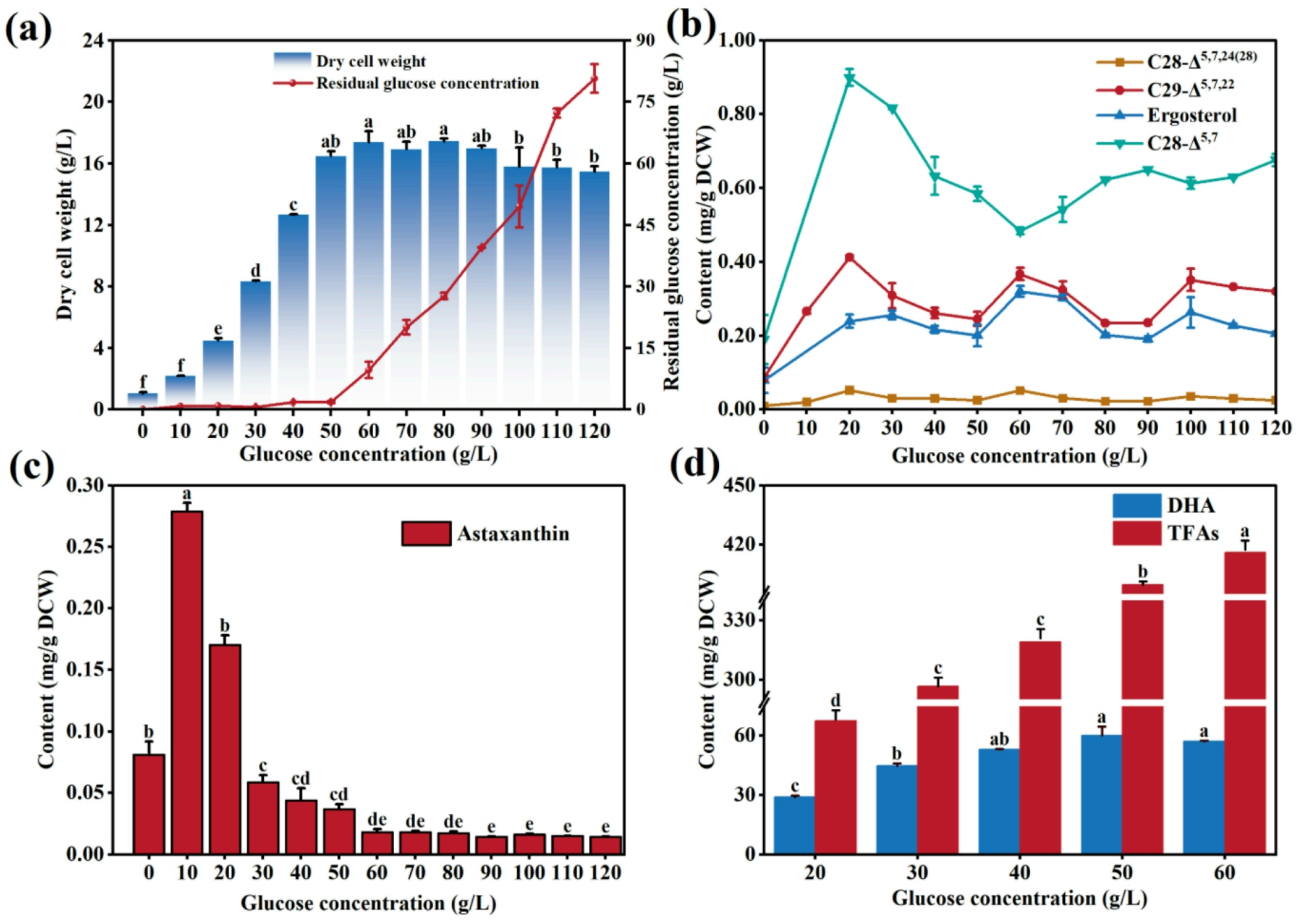


Figure 1

Residual glucose and dry cell weight (a), and the contents of $\Delta^{5,7}$-sterols (b), astaxanthin (c), DHA and TFAs (d) of *Schizochytrium* sp. S31 at different glucose concentrations.

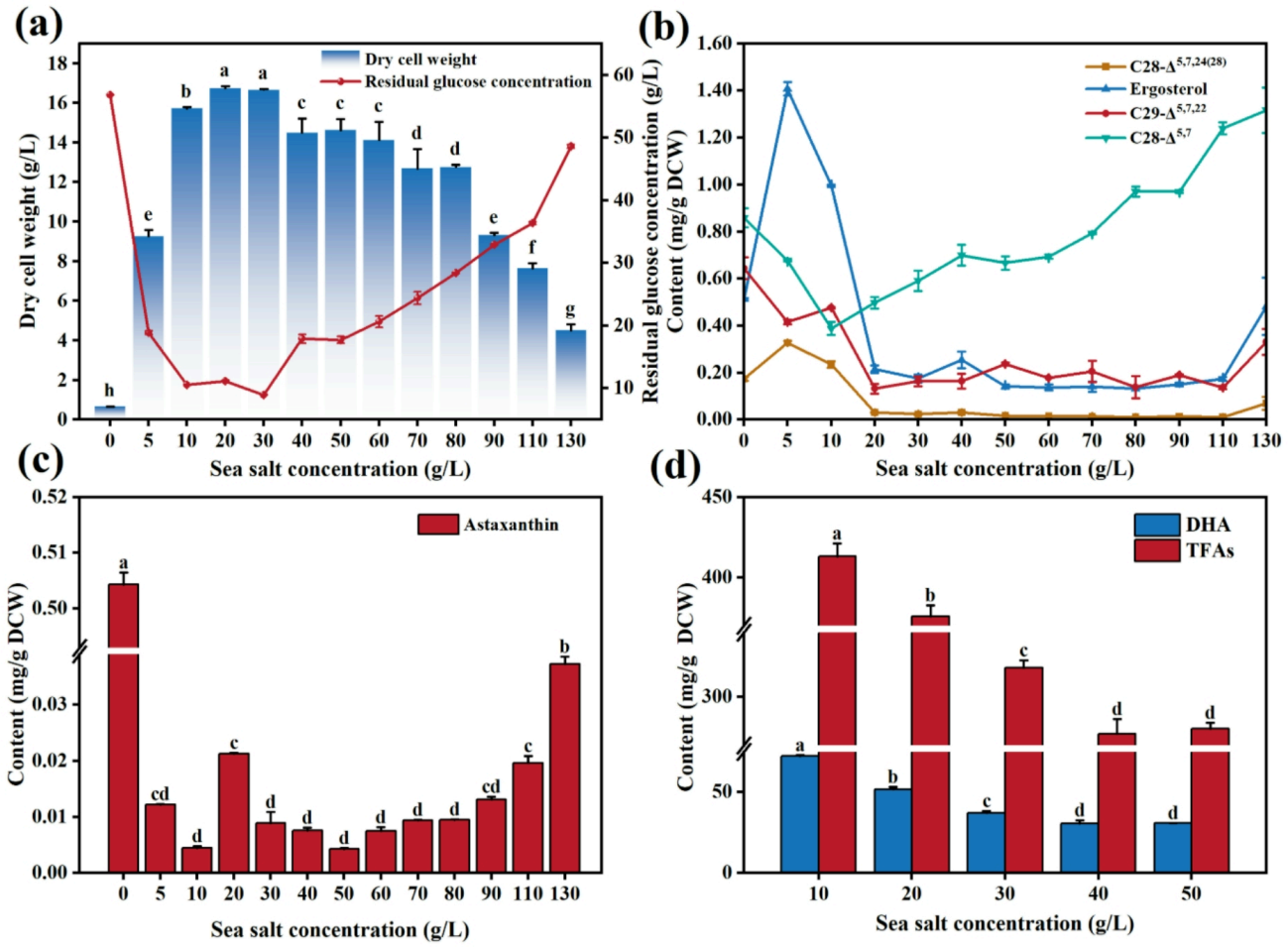


Figure 2

Residual glucose and dry cell weight (a), and the contents of $\Delta^{5,7}$-sterols (b), astaxanthin (c), DHA and TFAs (d) of *Schizochytrium* sp. S31 at different salt concentrations.

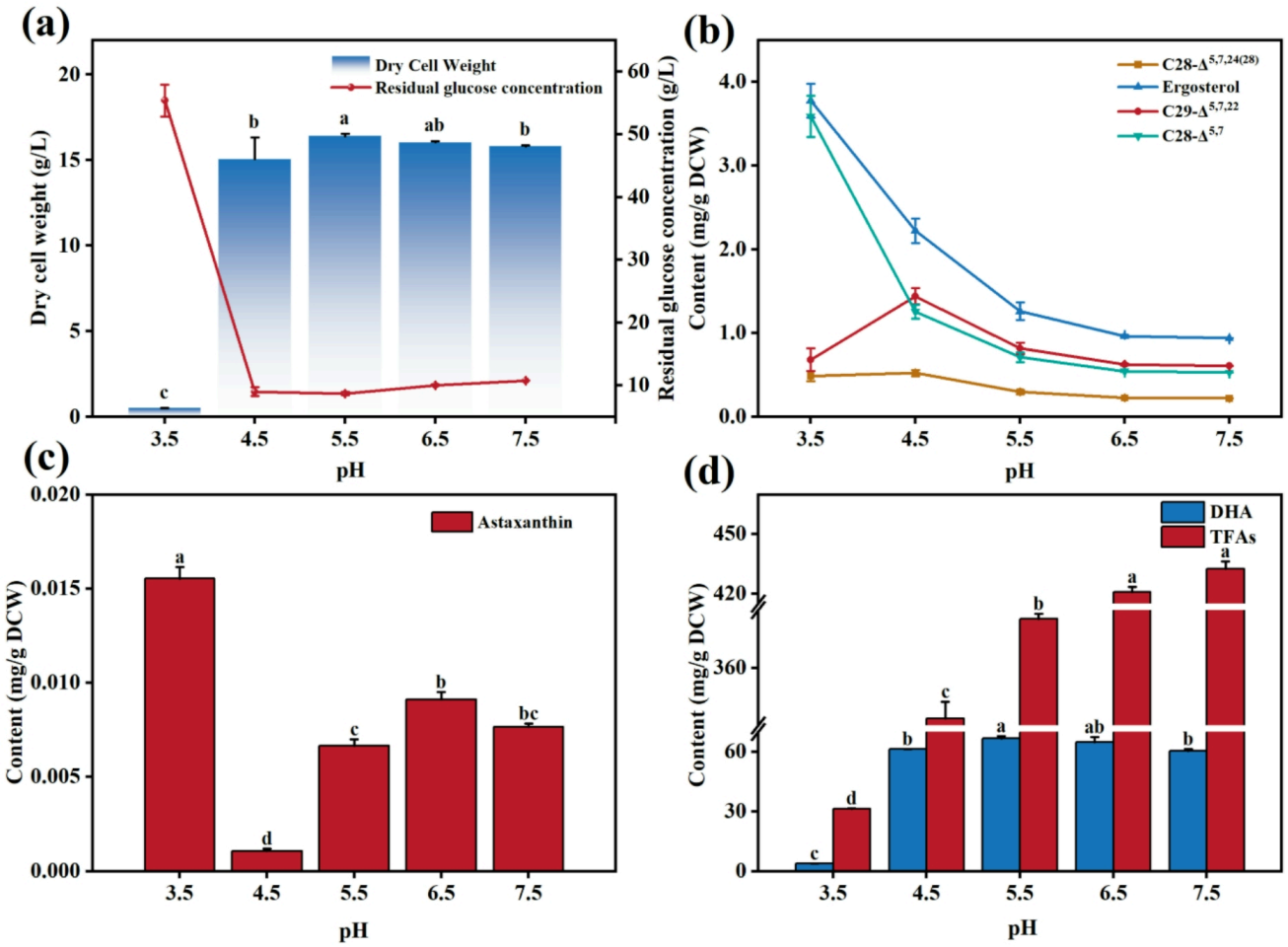


Figure 3

Residual glucose and dry cell weight (a), and the contents of $\Delta^{5,7}$-sterols (b), astaxanthin (c), DHA and TFAs (d) of *Schizochytrium* sp. S31 at different pH conditions.

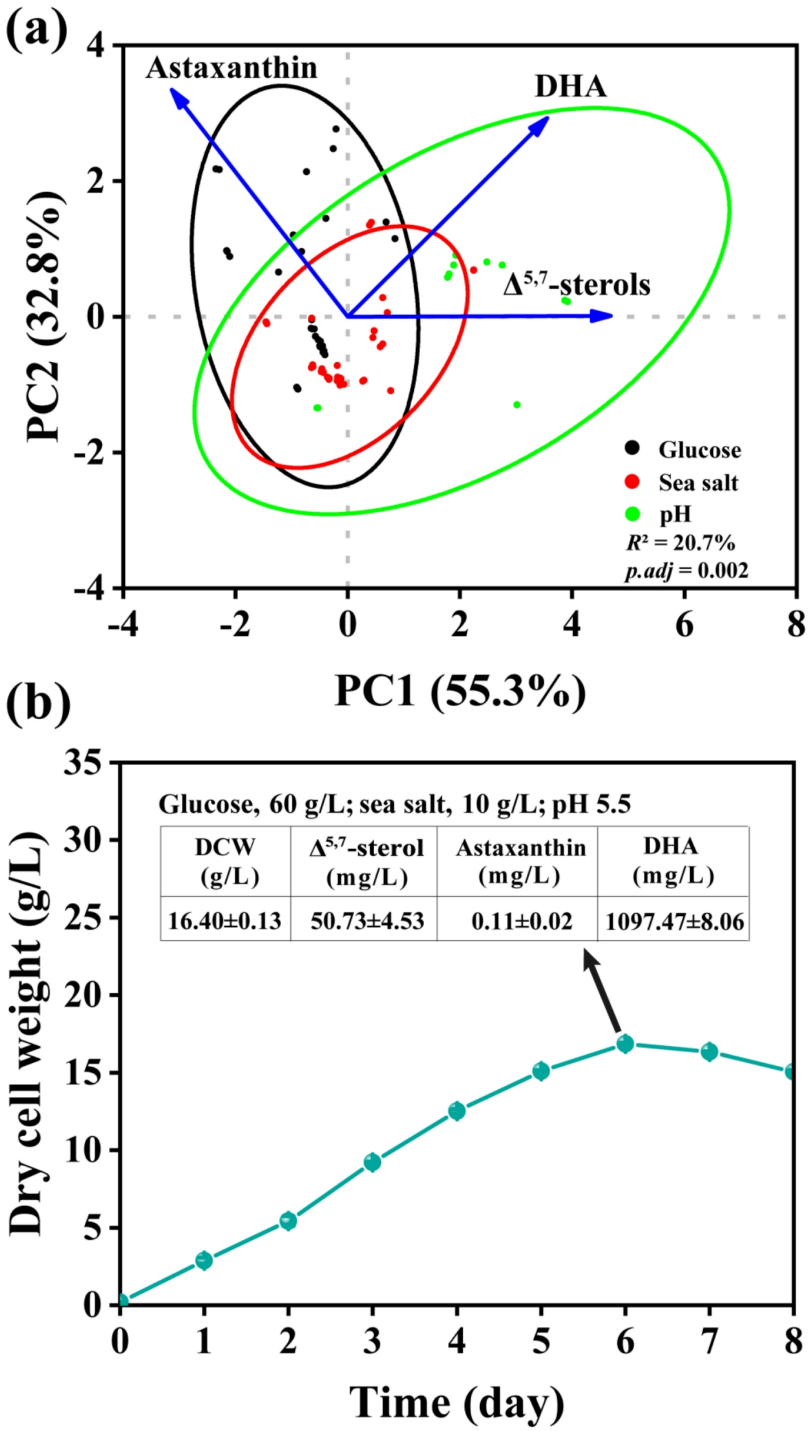


Figure 4

PCA of product yields under single-factor treatments and growth performance under combined optimal conditions in *Schizochytrium* sp. S31. a, PCA biplot of $\Delta^{5,7}$-sterols, astaxanthin and DHA yields across glucose, sea salt and pH gradients. Ellipses indicate 95% confidence intervals for each group. Inter-group differences were evaluated by PERMANOVA (R^2 = 0.207, P = 0.002); b, Time-course growth curve and

corresponding product yields under combined optimal conditions (60 g/L glucose, 10 g/L sea salt, pH 5.5). The inset table shows biomass and product yields on day 6 of cultivation.

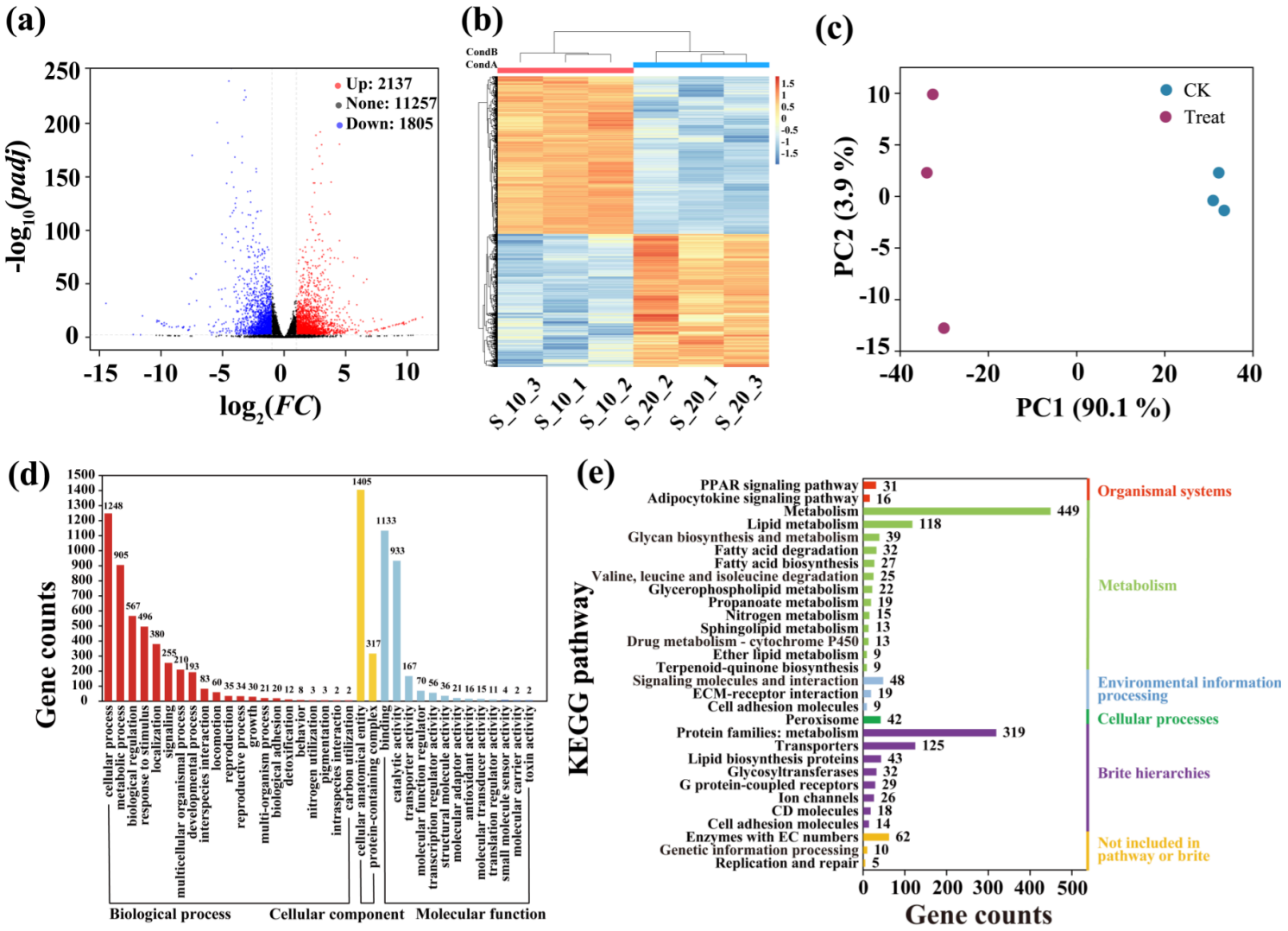


Figure 5

Transcriptomic analysis of *Schizochytrium* sp. S31 cultured under 10 g/L sea salt (treatment group, Treat) and 20 g/L sea salt (control group, CK). (a) Volcano plot displaying the distribution of differentially expressed genes (DEGs). Red dots represent significantly upregulated genes (2137), blue dots represent significantly downregulated genes (1805), gray dots represent genes without significant expression changes (11257). The screening thresholds were set as $|log_2FC| > 1$ and $padj < 0.01$. (b) Hierarchical clustering heatmap of all DEGs based on normalized gene expression values of six biological replicates. CondA corresponds to the treatment group and CondB corresponds to the control group. (c) Principal component analysis (PCA) of all sample transcriptome profiles. PC1 and PC2 explained 90.1% and 3.9% of the total variance respectively. (d) Bar chart showing the statistical distribution of DEGs across different KEGG pathway categories. (e) Gene Ontology (GO) functional classification of DEGs, which were divided into three major categories including Biological Process, Cellular Component and Molecular Function.

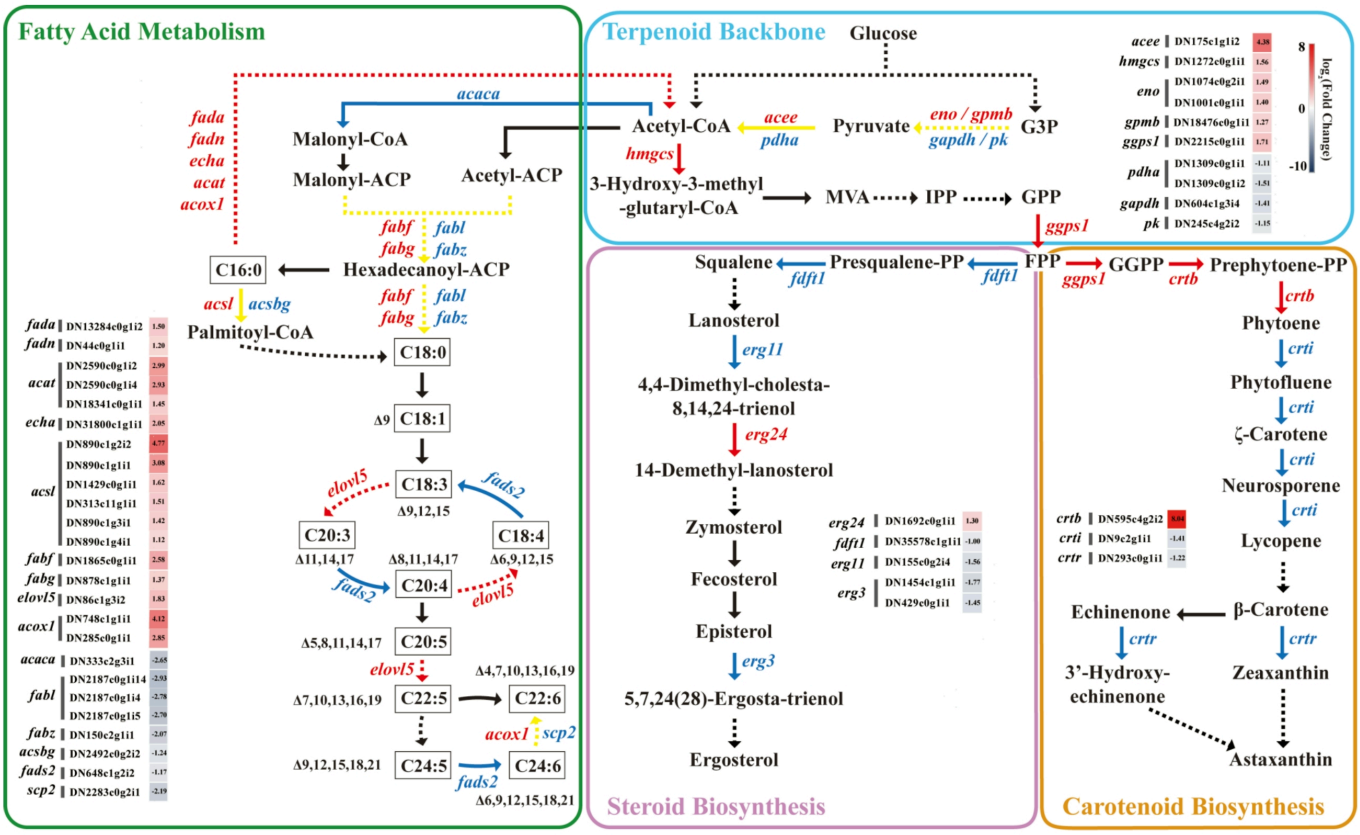


Figure 6

Schematic diagram of fatty acid metabolism, terpenoid backbone, sterol and carotenoid biosynthetic pathways in *Schizochytrium* sp. S31 under 10 g/L and 20 g/L sea salt conditions. Gene color gradients represent log_2 FC values, red for upregulated transcripts and blue for downregulated transcripts. MVA refers to the mevalonate pathway. Key DHA synthesis genes *ELOVL5* and *FADS2* are labeled. Fold changes stated in the text are raw values distinct from the log_2 FC shown here.

Supplementary Files

This is a list of supplementary files associated with this preprint. Click to download.

- SupplementarymaterialWJMB.docx